Electronic Supplementary Information

Mixed Functionalization Strategy on Indium-Organic Framework for Multiple Ions Detection and H_2O_2 Turn-on Sensing

Xin Jiang,[a] Ruiqing Fan,*[a] Xuesong Zhou,[a] Ke Zhu,[a] Tiancheng Sun,[a] Xubin Zheng,[a] Kai Xing,[a] Wei Chen,[a] and Yulin Yang*[a]

MIIT Key Laboratory of Critical Materials Technology for New Energy Conversion and Storage, School of Chemistry and Chemical Engineering, Harbin Institute of Technology, Harbin 150001, P. R. China
*corresponding author: Ruiqing Fan and Yulin Yang
E-mail: fanruiqing@hit.edu.cn and ylyang@hit.edu.cn

Experimental Section

Materials and Methods

All purchased reagents and solvents are commercially available and can be used without further purification. The various interference species (•OH, $^1O_2$, $O_2^{\bullet-}$, ROO•, NO•) were prepared according to the methods reported earlier.[1] FT-IR spectra (4000–400 cm^{-1}) were collected by ATR using a Nicolet Avatar-360 Infrared spectrometer. Powder X-ray diffraction (PXRD) patterns were recorded in the 2θ range of 5–50° using Cu Kα radiation with a Shimadzu XRD-6000 X-ray diffractometer. Scan electron microscope (SEM) images were recorded by Rili SU 8000HSD Series Hitachi New Generation Cold Field Emission SEM. UV-vis spectra were obtained on a Perkin-Elmer Lambda 20 spectrometer at room temperature. Elemental analyses were performed on a Perkin–Elmer 2400 automatic analyzer. The thermal analyses were performed on a ZRY-2P thermogravimetric analysis from 40 to 750°C with a heating rate of 10 °C·min^{-1} under a flow of air. XPS experiments were carried out on a RBD upgraded PHI-5000C ESCA system (Perkin Elmer) with Mg Kα radiation (hv = 1253.6 eV). All the fluorescence spectra were recorded with Edinburgh FLS 920 fluorescence spectrometer equipped with a Peltier-cooled Hamamatsu R928 photomultiplier tube. An Edinburgh Xe900 450 W xenon arc lamp was used as an exciting light source. The average fluorescence lifetime $<\tau>$ of **In1-NH_2** was calculated according to the following equation: $<\tau> = \frac{\tau_1^2 A_1\% + \tau_2^2 A_2\%}{\tau_1 A_1\% + \tau_2 A_2\%}$. The fluorescent quantum yield was measured with a G8 integration sphere (GMP SA, Switzerland) from the Edinburgh FLS 920 fluorescence spectrometer.

Single-Crystal X-Ray Crystal Structure Determination

The X-ray diffraction data of **In1-NH_2** was collected on a Rigaku R-AXIS RAPID IP diffractometer equipped with graphite-monochromated Mo Kα radiation (λ = 0.71073 Å) at room temperature. The structure of **In1-NH_2** was solved by direct method and refined on F^2 by the full-matrix least squares using the SHELXTL-97 crystallographic software. Anisotropic thermal parameters were refined to all of the non-hydrogen atoms. The hydrogen atoms were held in calculated ideal positions on carbon atoms and nitrogen atoms in ligands and that were directly included in the molecular formula on water molecules. The amino group can be in any of the four equivalent positions. The chemical formulas were determined by the combination of single crystal data, TGA results and elemental analysis. The CCDC 2008844 contains the crystallographic data **In1-NH_2** of this paper. These data can be obtained free of charge at www.ccdc.cam.ac.uk/deposit. Crystal structure data and details of the data collection and the structure refinement are listed as Table S1, selected bond lengths and bond angles of **In1-NH_2** are listed as Table S2.

Synthesis of In1-NH_2

A mixture of $In(NO_3)_3$•H_2O (47.82 mg，0.15 mmol) and H_2BDC-NH_2 (18.12 mg，0.10 mmol) was dissolved in H_2O solvent (8.00 mL) in a Teflon-lined stainless steel autoclave (23 mL), which was heated for 72 h at 120°C. And then after the mixture was slowly cooled down to the room temperature, yellow crystals with block shape were obtained (yield: 56.3%, based on indium metal). Anal. calcd (%) for

$C_8H_6InO_5N$ (Mr = 310.96): C, 30.89; H, 1.93; N, 4.51. Found: C, 31.91; H, 1.98; N, 4.46. IR data (ATR, cm^{-1}): 3620 (w), 3474 (s), 3374 (s), 2633 (w), 2360 (m), 2341 (v), 1625 (w), 1560 (s), 1493 (m), 1428 (s), 1383 (s), 1334 (w), 1300 (w), 1255 (s), 1231 (w), 1157 (w), 1120 (w), 1018 (w), 893 (m), 865 (m), 827 (m), 764 (s), 696 (w), 580 (w), 525 (w), 432 (w) (Fig. S4).

Synthesis of PBA-In1

PBA-In1 was generated based on the classical method for preparing amides. Firstly, CPBA (0.2 g, 4-carboxyl phenylboronic acid) was dissolved in a beaker with 20 mL DMSO. Then, EDC (0.04 g, 1-(3-dimethyl aminopropyl)-3-ethyl carbodiimide hydrochloride) and NHS (0.08 g, N-hydroxy succinimide) were added into the solution in order, followed by ultrasonic treatment for 20 minutes. Subsequently, the fresh sample of **In1-NH_2** (0.1 g) was added into the solution, and a further ultrasonic treatment was carried out for 30 minutes to realize a uniform mixture. After the reaction at 37°C for 36 h, the **PBA-In1** sample was obtained by washing the product with ethanol and the deionized water for four times, and drying at 100°C. IR data (ATR, cm^{-1}): 3595 (w), 3302 (w), 3116 (m), 2360 (m), 2341 (v), 1683 (s), 1619 (w), 1543 (s), 1420 (s), 1373 (s), 1325 (m), 1242 (m), 1205 (w), 1156 (s), 1127 (w), 1095 (w), 1077 (w), 1051 (m), 996 (w), 951 (w), 887 (m), 792 (m), 759 (s), 694 (w), 566 (w), 494 (s) (Fig. S4).

Fluorescent sensing experiments

Fresh sample of **In1-NH_2** (10 mg) was ground and added into the deionized water

(100 mL) followed by the ultrasonic treatment for 10 minutes to form a stable aqueous suspension.

For the heavy metal ions detection, the fluorescence response of **In1-NH_2** to various metal ions were firstly investigated (each analyte concentration was 1 mM). Obviously, Fe^{3+}, Cu^{2+} and Pb^{2+} could greatly quench the fluorescence of **In1-NH_2**. Subsequently, the fluorescence response of **In1-NH_2** to Fe^{3+}, Cu^{2+} and Pb^{2+} was further investigated (the concentration ranged from 0 to 0.5 mM). And **In1-NH_2** might be a good candidate to monitor heavy metal ions. All the fluorescence emission spectrum measured at an excitation wavelength of 350 nm.

For the ClO^- detection, equal volume ClO^- aqueous solution with different concentrations were mixed with 2 mL above **In1-NH_2** suspension, and the concentration of ClO^- ranged from 0 to 0.32 mM. Subsequently, the concentration dependent fluorescence emission spectra were measured under the excitation wavelength of 350 nm. In order to evaluate the detection selectivity, different competitive ions (such as $C_2O_4^{2-}$, CH_3COO^-, Br^-, Cl^-, F^-, I^-, ClO_4^-, NO_3^-, SO_3^{2-} and SO_4^{2-}), were separately added to the 2 mL above solution (each analyte concentration was 1 mM). And then, all the fluorescence emission spectra of these mixtures were measured before and after further adding 0.32 mM ClO^- solution.

The as-prepared **PBA-In1** (10 mg) was ground and added into HEPES buffer solution (100 mL, 10 mM, pH 7.4) followed by the ultrasonic treatment for 10 minutes to form a stable aqueous suspension.

For the H_2O_2 detection, equal volume H_2O_2 aqueous solutions with different concentrations were added into 2 mL above **PBA-In1** suspension. After 10 minutes of ultrasonic treatment, the concentration dependent fluorescence emission spectra were measured under the excitation wavelength of 350 nm. Furthermore, to evaluate the detection selectivity, different interferences [including hydroxyl radical (•OH), singlet oxygen ($^1O_2$), superoxide anion ($O_2^{\bullet-}$), alkyl peroxide (ROO•), nitric oxide (NO•)] were respectively added into 2 mL above **PBA-In1** suspension (each analyte concentration was 80 μM). Subsequently, these mixtures were thoroughly stirred for three minutes and form stable suspensions for measuring fluorescence emission spectra at an excitation wavelength of 350 nm. And then, all the fluorescence emission spectra of these mixtures were measured again after further adding equal H_2O_2 solution.

Table S1. Crystallographic data and structural refinements of **In1-NH_2**.

Identification code	**In1-NH_2**
Empirical formula	$C_8H_6InNO_5$
CCDC	2008844
Formula weight	310.96
Crystal system	Orthorhombic
Space group	Imma
a (Å)	18.2629(6)
b (Å)	7.1950(3)
c (Å)	12.0467(4)
α (˚)	90.00
β (˚)	90.00
γ (˚)	90.00
V ($Å^3$)	1582.96(10)
Z	4
Dc/(g cm^{-3})	1.305
μ (Mo Kα)/ (mm^{-1})	1.493
F(000)	600
θ range (°)	3.298–24.982
Limiting indices	$-21 \le h \le 20$
	$-6 \le k \le 8$
	$-13 \le l \le 14$
Data/Restraints/Parameters	751 / 6 / 48
GOF on F^2	1.162
[a]R_1	0.0500
[b]wR_2	0.1355
R1	0.0605
wR2	0.1438
Largest diff peak, hole (e $Å^{-3}$)	1.972, -1.087

[a] $R_1 = \sum||F_o| - |F_c||/ \sum|F_o|$; [b] $wR_2 = [\sum[w (F_o^2 - F_c^2)^2] / \sum[w (F_o^2)^2]]^{1/2}$.

Table S2. Selected bond lengths (Å) and bond angles (°) of **In1-NH_2**.

In1-NH_2			
In(1)-O(1)	2.084(5)	In(1)-O(1)#1	2.084(5)
In(1)-O(2)	2.141(5)	In(1)-O(2)#1	2.141(5)
In(1)-O(2)#2	2.141(5)	In(1)-O(2)#3	2.141(5)
O(1)-In(1)-O(1)#1	180.0	O(1)-In(1)-O(2)#2	88.2(2)
O(1)#1-In(1)-O(2)#2	91.8(2)	O(1)-In(1)-O(2)#3	91.8(2)
O(1)#1-In(1)-O(2)#3	88.2(2)	O(2)#2-In(1)-O(2)#3	180.0(3)
O(1)-In(1)-O(2)#1	91.8(2)	O(1)#1-In(1)-O(2)#1	88.2(2)
O(2)#2-In(1)-O(2)#1	86.3(4)	O(2)#3-In(1)-O(2)#1	93.7(4)
O(1)-In(1)-O(2)	88.2(2)	O(1)#1-In(1)-O(2)	91.8(2)
O(2)#2-In(1)-O(2)	93.7(4)	O(2)#3-In(1)-O(2)	86.3(4)
O(2)#1-In(1)-O(2)	180.0		

Symmetry transformations used to generate equivalent atoms:

#1 -x,-y,-z+1 #2 -x,y,z #3 x,-y,-z+1 #4 -x,-y-1/2,z #5 x,-y+1/2,z #6 -x+1/2,y+0,-z+1/2

Table S3. Standard deviation and limit of detection calculation of **In1-NH_2**.

No.	**Fluorescence Intensity (I_{429}) of In1-NH_2 in H_2O**	**I_0/I-1**
1	3139.34 a.u.	0
2	3123.58 a.u.	0.00505
3	3136.63 a.u.	0.00086
4	3133.52 a.u.	0.00186
5	3129.08 a.u.	0.00328
Standard Deviation (σ)	--	0.00158

Table S4. Standard deviation and limit of detection calculation of **PBA-In1**.

No.	**Fluorescence Intensity (I_{429}) of PBA-In1 in H_2O**	**I/I_0**
1	997.48 a.u.	1
2	993.02 a.u.	0.99553
3	994.77 a.u.	0.99728
4	998.83 a.u.	1.00135
5	996.56 a.u.	0.99908

Standard Deviation (σ)	--	0.00204

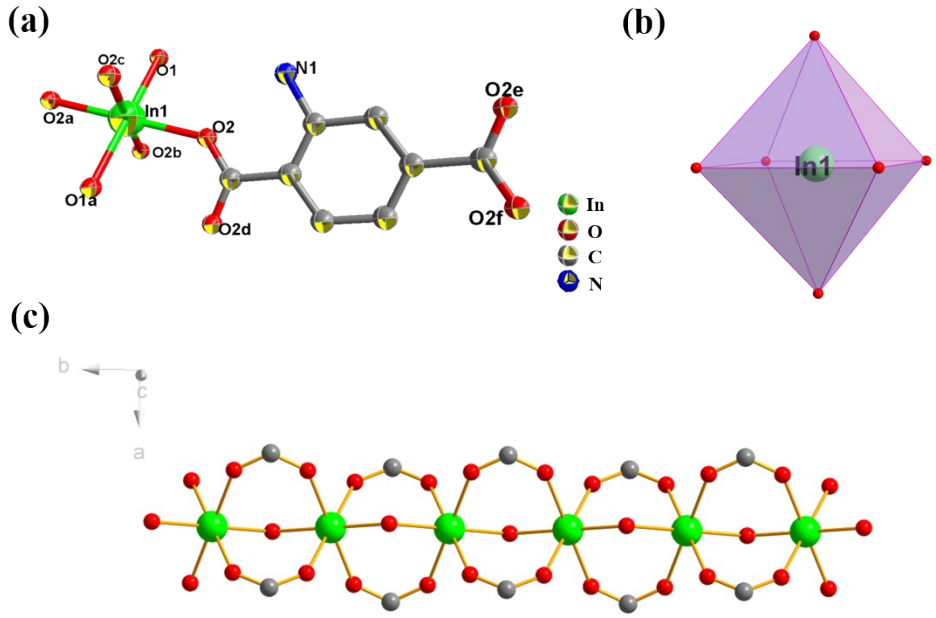

Fig. S1. (a) The asymmetric structural unit of **In1-NH$_2$**; (b) Octahedron geometry of In^{3+} in **In1-NH$_2$**. (c) The 1D chain along the *b* axis.

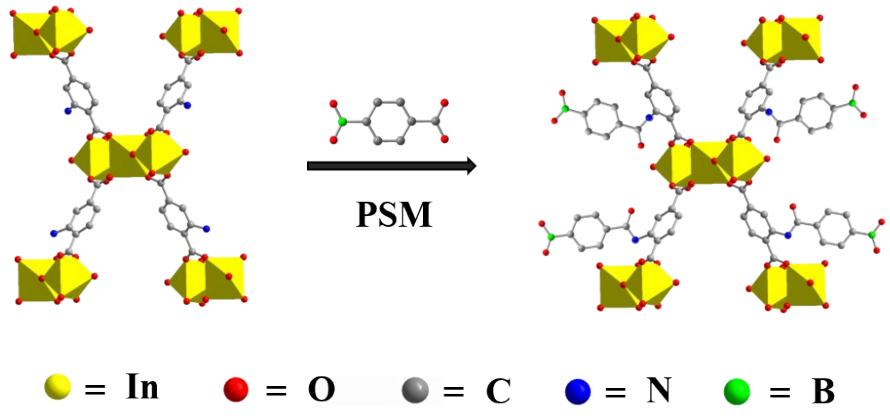

Scheme S1. Synthesis Process of **PBA-In1**.

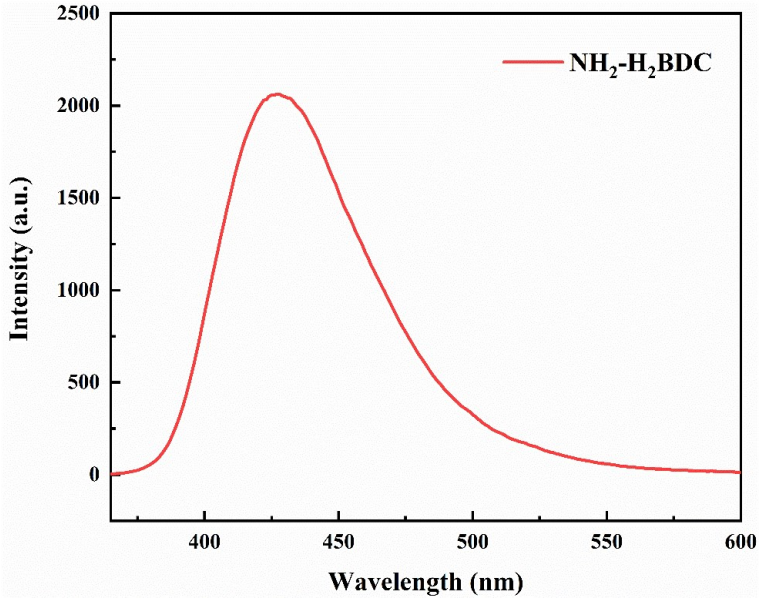

Fig. S2. Fluorescence emission spectra of **NH_2-H_2BDC** under excitation at 350 nm.

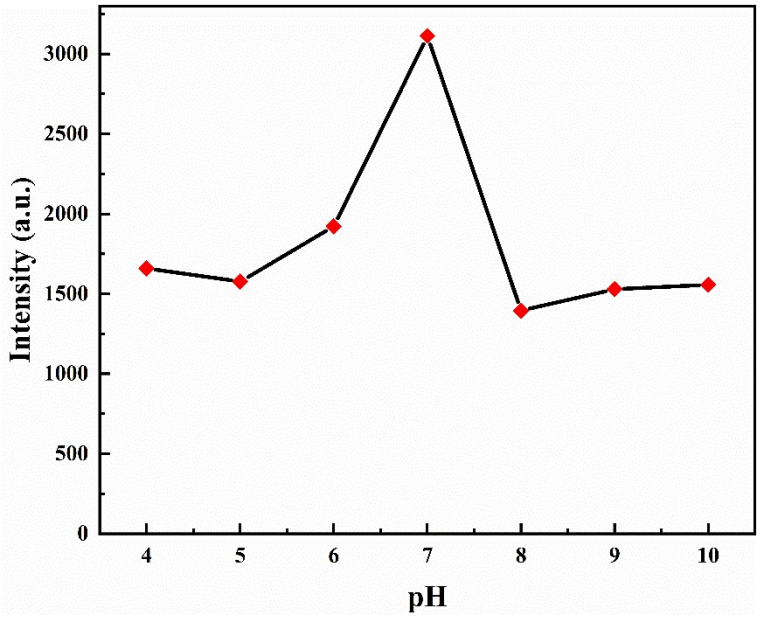

Fig. S3. The effect of different pH on thefluorescence intensity of **In1-NH_2**.

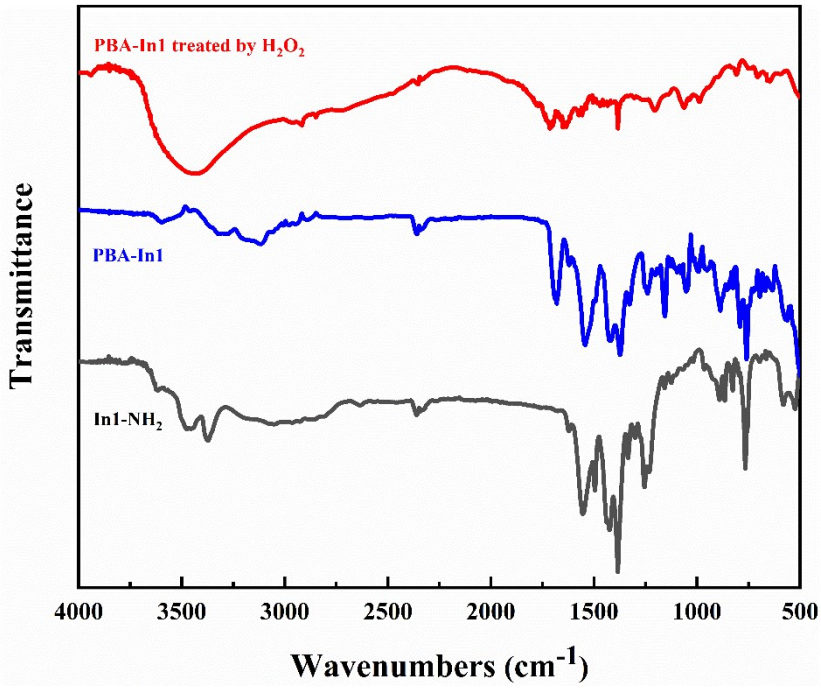

Fig. S4. FT-IR spectra of **In1-NH_2**, **PBA-In1**, and **PBA-In1** treated by H_2O_2.

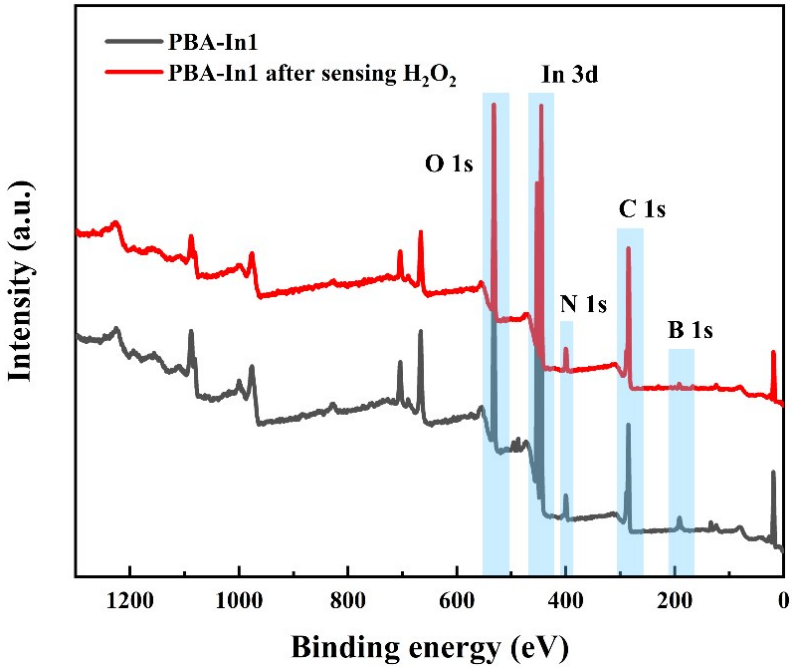

Fig. S5. XPS spectra of **PBA-In1** and **PBA-In1** treated by H_2O_2.

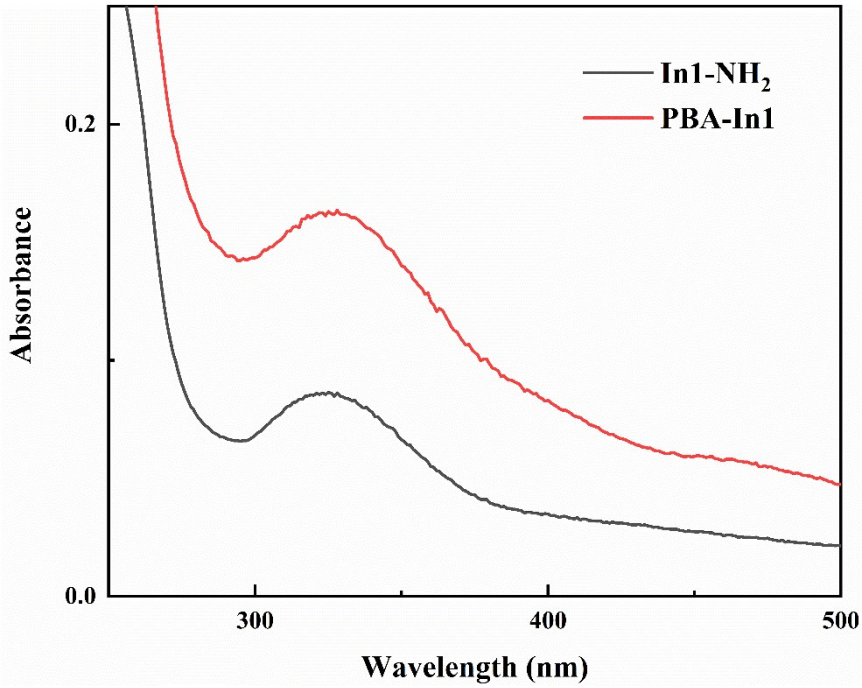

Fig. S6. UV-vis absorption spectra of the pure **In1-NH$_2$** and **PBA-In1** composites.

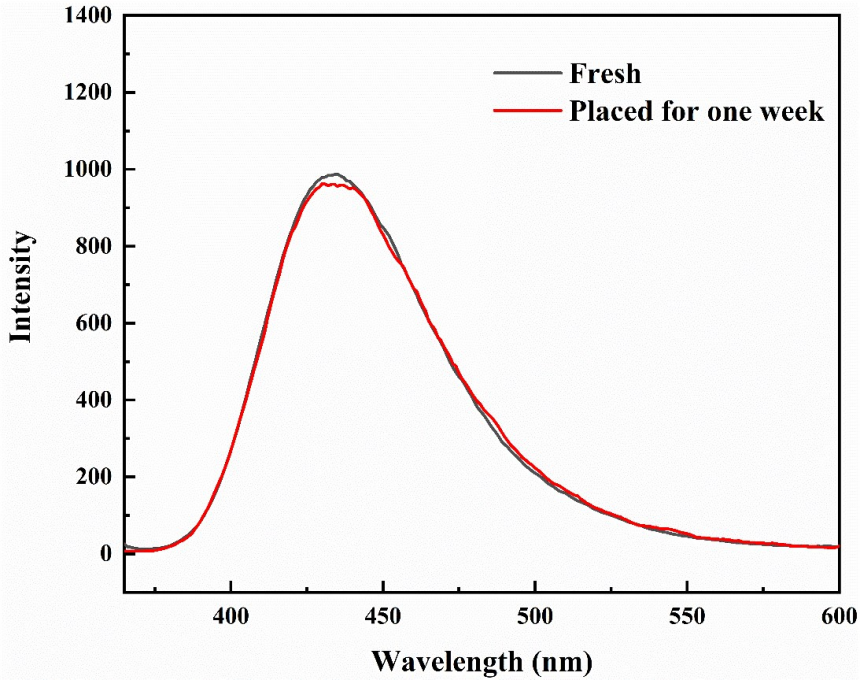

Fig. S7. Fluorescence emission spectrum of the **PBA-In1** and placed for one week under excitation at 350 nm.

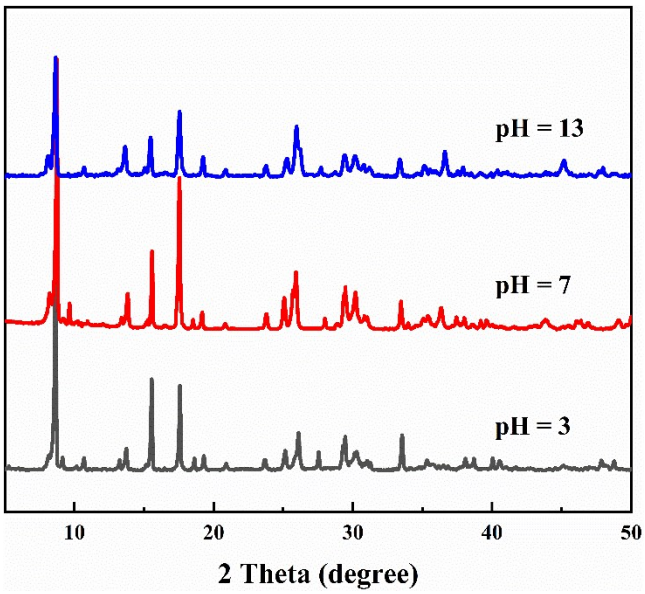

Figure S8. PXRD patterns of **PBA-In1** treated by water, acidic and basic aqueous solutions.

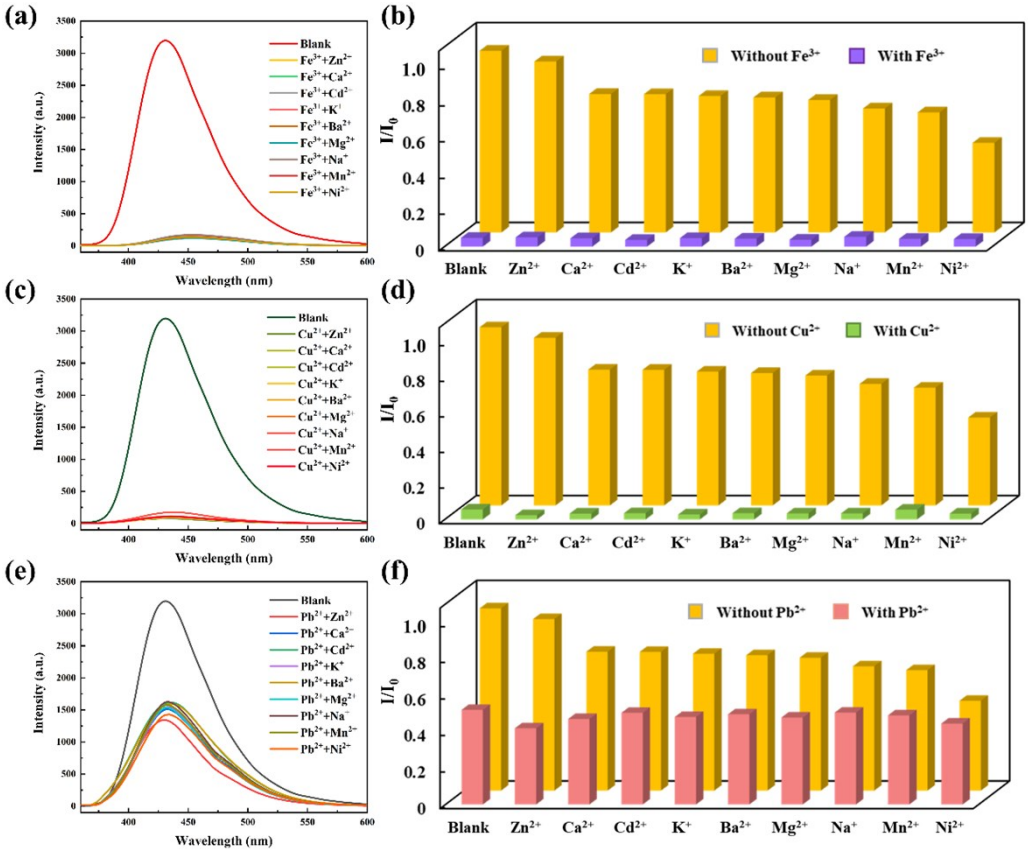

Fig. S9. (a, c and e) Emission spectra of **In1-NH_2** treated by Fe^{3+}, Cu^{2+} and Pb^{2+} with coexisting cations, respectively. (b, d and f) The anti-interference ability of probe **In1-NH_2** towards various interferences.

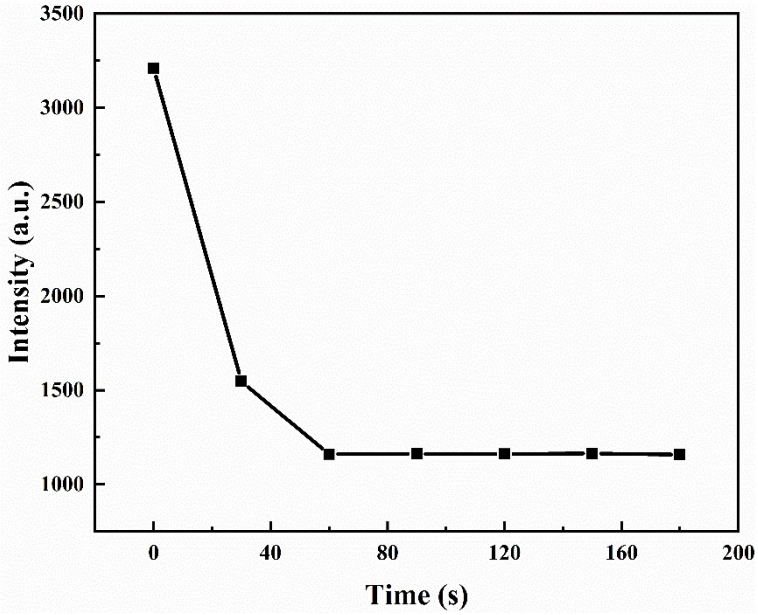

Fig. S10. The change of fluorescence intensity of **In1-NH$_2$** towards addition of ClO^- (0.16 mM).

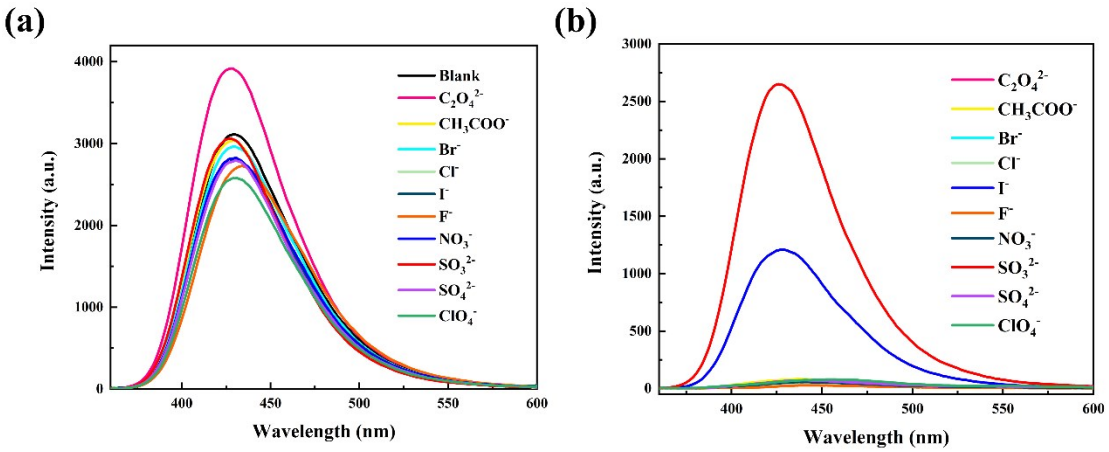

Fig. S11. (a) Emission spectra of **In1-NH$_2$** with various anions. (b) Emission spectra of **In1-NH$_2$** treated by ClO^- with coexisting anions.

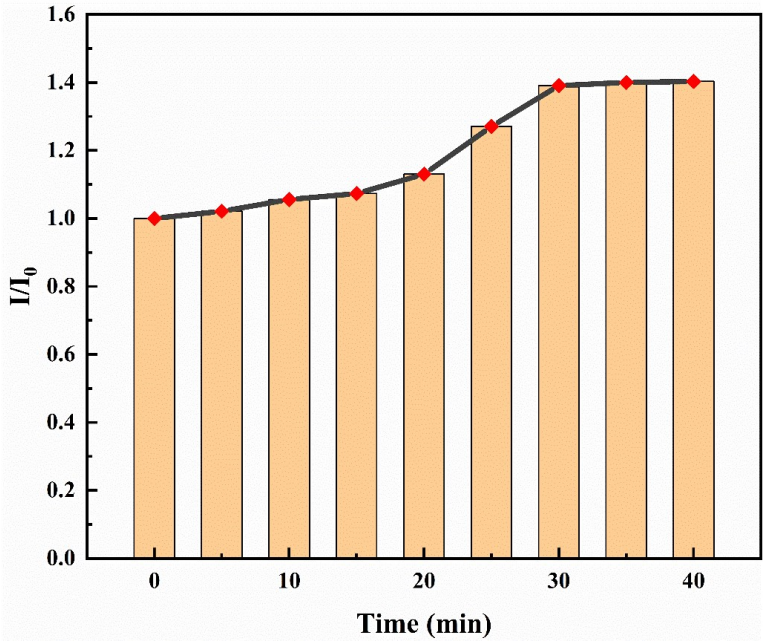

Fig. S12. Fluorescence intensity ratio of the **PBA-In1** towards addition of H_2O_2 (25 μM).

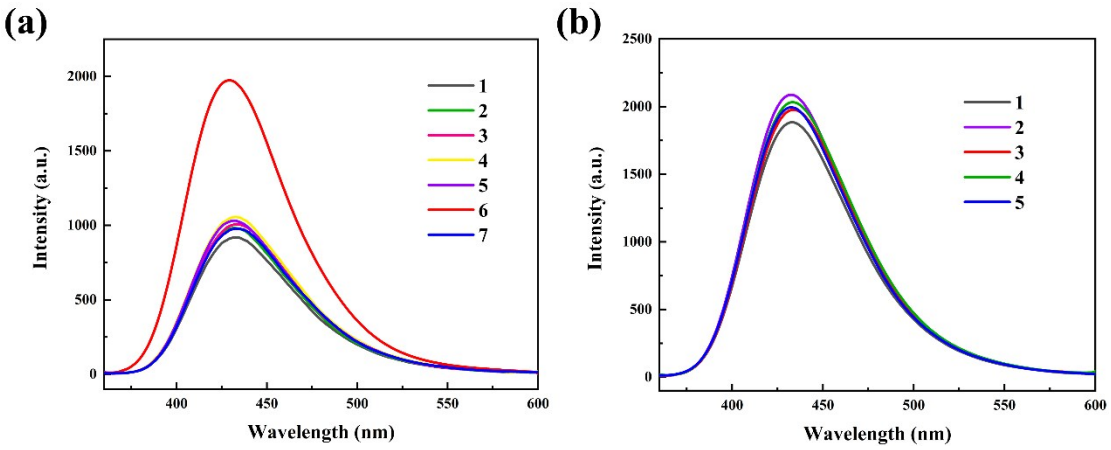

Fig. S13. (a) Emission spectra of **PBA-In1** with various interference species (1: •OH; 2: $^1O_2$; 3: $O_2^{\bullet-}$; 4: ROO•; 5: NO•; 6: H_2O_2; 7: origin;). (b) Emission spectra of **PBA-In1** treated by H_2O_2 with coexisting interferences 1~5.

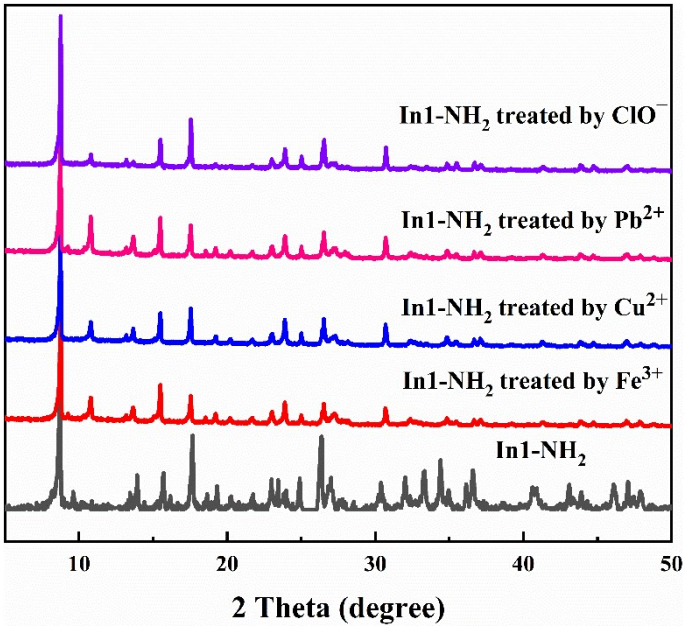

Fig. S14. PXRD patterns of **In1-NH$_2$** and **In1-NH$_2$** treated by different heavy metal ions and ClO^-.

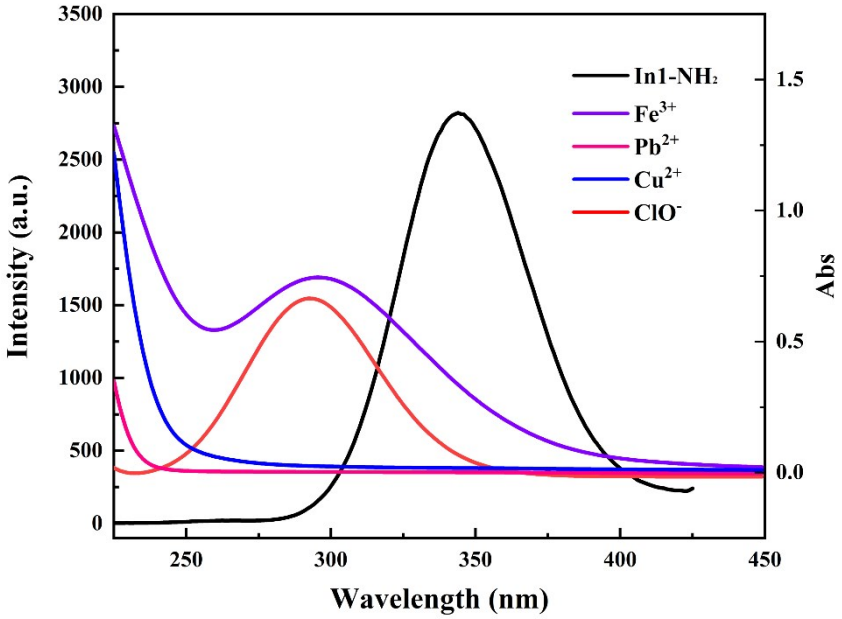

Fig. S15. UV-Vis absorption spectra of various heavy metal ions and ClO^- and the excitation spectrum of **In1-NH$_2$**.

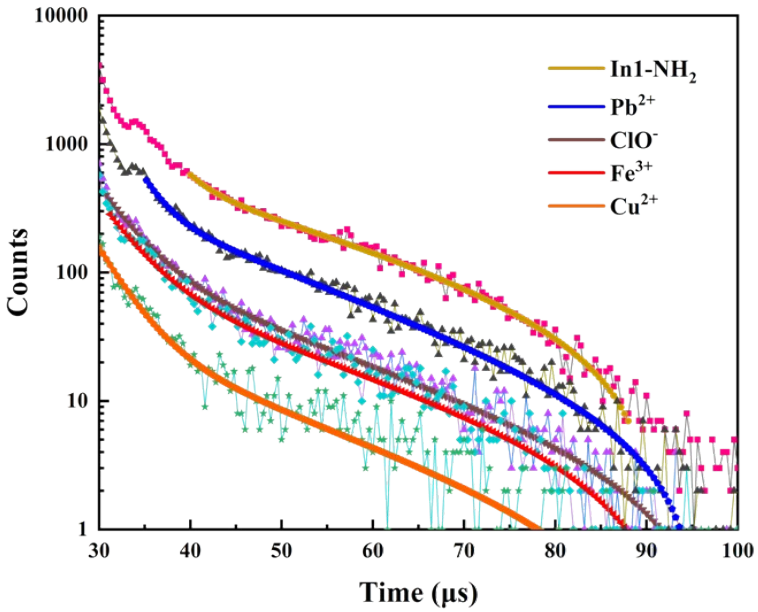

Fig. S16. The fluorescent lifetime of **In1-NH$_2$** and **In1-NH$_2$** treated by different heavy metal ions and ClO^-.

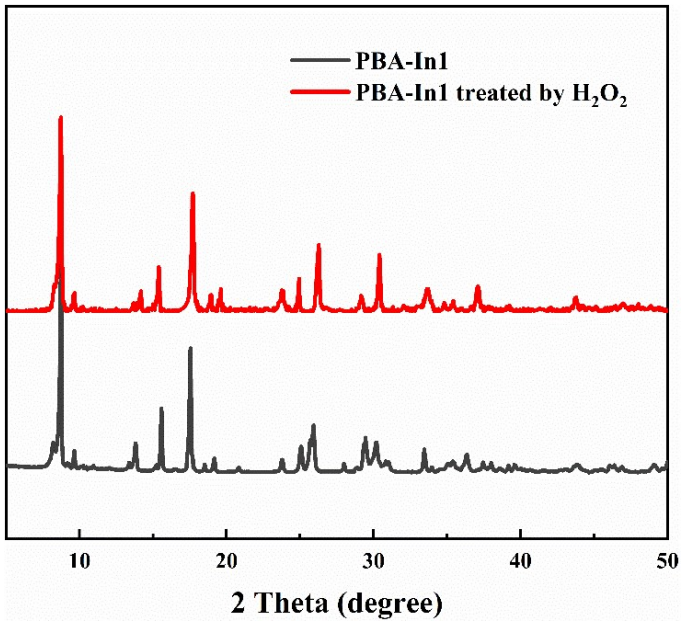

Fig. S17. PXRD patterns of **PBA-In1** and **PBA-In1** treated by H_2O_2.

Table S5. Comparison of the limit of detection (LOD) for the heavy metal ions sensing by materials reported till date using different analytical methods.

No.	Material	Limit of Detection (LOD) (μM)	Analytical Method	Reference
1	MIL-101-NH_2	1.80 μM for Fe^{3+}; 1.60 μM for Cu^{2+}; 5.20 μM for Pb^{2+}	fluorescence	[2]
2	pyridine-2,6-dicarboxamide	1.49 μM for Cu^{2+}; 2.31 μM for Pb^{2+}	fluorescence	[3]
3	QMNPS	2.0 μM for Cu^{2+}; 1.6 μM for Pb^{2+}	NMR	[4]
4	APA-Rh	0.91 μM for Fe^{3+}; 1.04 μM for Cu^{2+}	fluorescence	[5]
5	C1	0.41 μM for Fe^{3+}; 0.293 μM for Cu^{2+}	colorimetry	[6]
6	N-CQDs	0.173 μM for Fe^{3+}; 0.16 μM for Cu^{2+}	fluorescence	[7]
7	In1-NH_2	0.11 μM for Fe^{3+}; 0.14 μM for Cu^{2+}; 1.15 μM for Pb^{2+}	fluorescence	This work

QMNPs = quercetin-coated Fe_3O_4 nanoparticles; APA-Rh = arylpropenone azo dye appended rhodamine-based dual chemosensor; C1 = indole[2,3-a]carbazole-based Schiff base; N-CQDs = nitrogen-doped carbon quantum dots.

Table S6. Comparison of the LOD for the ClO^- sensing by materials reported till date using different analytical methods.

No.	Material	Limit of Detection (LOD) (μM)	Analytical Method	Reference
1	CGB	10.67	fluorescence	[8]
2	BK	7.65	fluorescence	[9]
3	PYCN	2.83	fluorescence	[10]
4	N-CQDs	1.47	fluorescence	[11]
5	NCS-BOD-OCH_3	1.15	fluorescence	[12]
6	P1	0.92	fluorescence	[13]
7	In1-NH_2	0.64	fluorescence	This work

CGB = N-(1,3-dioxo-1H-benzo[de]isoquinolin-2(3H)-yl)-3-hydroxy-2-naphthamide; BK = (E)-2-((acridine-9-ylimino)methyl)-N-benzhydrylhydrazine-1-carbothioamide; PYCN = pyrene-based Schiffbase derivative; N-CQDs = nitrogen-doped carbon quantum dots; NCS-BOD-OCH_3 = near-infrared BODIPY-based probe; P1 = two-photon polysiloxane-based reversible probe.

Table S7. Comparison of the LOD for the H_2O_2 sensing by materials reported till date using different analytical methods.

No.	Material	Limit of Detection (LOD) (μM)	Analytical Method	Reference
1	FePt-Au HNPs	12.33	fluorescence	[14]
2	Co-MOF	3.76	electrochemistry	[15]
3	Hemin@HKUST-1	2.0	chemiluminescence	[16]
4	Fe@PCN-224	1.6	colorimetry	[17]
5	ZIF-67/rGO/GCE	1.57	electrochemistry	[18]
6	3AMBA-HRP-SWCNT	0.85	fluorescence	[19]
7	PBA-In1	0.42	fluorescence	This work

FePt-Au HNPs = FePt-Au ternary metallic hybrid nanoparticles; rGO = reduced graphene oxide, GCE = glassy carbon electrode; 3AMBA = 3-aminophenylboronic acid, HRP = horseradish peroxidase, SWCNT = single-wall carbon nanotubes.

REFERENCES

1 M. Kim, S. K. Ko, H. Kim, I. Shin and J. Tae, *Chem Commun*, 2013, **49**, 7959-7961.
2 S.-W. Lv, J.-M. Liu, C.-Y. Li, N. Zhao, Z.-H. Wang and S. Wang, *Chem Eng J,* 2019, **375**, 122111.
3 H. Rahimi, R. Hosseinzadeh and M. Tajbakhsh, *J Photoch and Photobio A,* 2021, **407**, 113049.
4 W. Jiang, S. Yang, X. Sun, W. Lu, D. Jiang, L. Xu, H. Xu, B. Gao, M. Ma and F. Cao, *Anal Methods,* 2018, **10**, 2494-2502.
5 A. Sağırlı and E. Bozkurt, *J Photoch and Photobio A,* 2020, **403**, 112836.
6 Z. E. Chen, X. F. Zang, M. Yang and H. Zhang, *Spectrochim. Acta, Part A,* 2020, **234**, 118236.
7 C. Hu, Y. Zhu and X. Zhao, *Spectrochim. Acta, Part A,* 2021, **250**, 119325.
8 S. C. Lee and C. Kim, *Inorg. Chem. Commun,* 2019, **108**, 107545.
9 S. C. Lee, S. Park, H. So, G. Lee, K. T. Kim and C. Kim, *Sensors (Basel)*, 2020, **20**, 4764.
10 Y. Yang, C.-Y. Gao, J. Chen, N. Zhang and D. Dong, *Anal Methods,* 2016, **8**, 805-809.
11 Q. Jiang, Y. jing, Y. Ni, R. Gao and P. Zhou, *Microchemical Journal*, 2020, **157**, 105111.
12 B. X. Shen, Y. Qian, Z. Q. Qi, C. G. Lu, Q. Sun, X. Xia and Y. P. Cui, *J Mater Chem B*, 2017, **5**, 5854-5861.
13 Y. Zuo, Y. Zhang, B. Dong, Z. Gou, T. Yang and W. Lin, *Anal Chem*, 2019, **91**, 1719-1723.
14 Y. Ding, B. Yang, H. Liu, Z. Liu, X. Zhang, X. Zheng and Q. Liu, *Sens. Actuators, B,* 2018, **259**, 775-783.
15 L. Yang, C. Xu, W. Ye and W. Liu, *Sens. Actuators, B,* 2015, **215**, 489-496.
16 F. Luo, Y. Lin, L. Zheng, X. Lin and Y. Chi, *ACS Appl Mater Interfaces,* 2015, **7**, 11322-11329.
17 T. Li, P. Hu, J. Li, P. Huang, W. Tong and C. Gao, *Colloid Surface A,* 2019, **577**, 456-463.
18 Y. Dong and J. Zheng, *Sens. Actuators, B,* 2020, **311**, 127918.
19 Y. Qiao, R. Zhao, M. Zhang, H. Zhang, Y. Wang and P. Hu, *RSC Adv*, 2019, **9**, 2258-2267.